T2R2 東京科学大学 リサーチリポジトリ
Science Tokyo Research Repository

論文 / 著書情報
Article / Book Information

Title	Development of a 20-M-Long Giacometti Arm with Balloon Body Based on Kinematic Model with Air Resistance
Authors	Masashi Takeichi, Koichi Suzumori, Gen Endo, Hiroyuki Nabae
Citation	Proceedings of 2017 IEEE/RSJ International Conference on Intelligent Robots and Systems, Vol. , No. , pp. 2710-2716
Pub. date	2017, 9
Copyright	(c) 2017 IEEE. Personal use of this material is permitted. Permission from IEEE must be obtained for all other uses, in any current or future media, including reprinting/republishing this material for advertising or promotional purposes, creating new collective works, for resale or redistribution to servers or lists, or reuse of any copyrighted component of this work in other works.
DOI	http://dx.doi.org/10.1109/IROS.2017.8206097
Note	This file is author (final) version.

Powered by T2R2 (Science Tokyo Research Repository)

Development of a 20-m-long Giacometti Arm with Balloon Body Based on Kinematic Model with Air Resistance

Masashi Takeichi, Koichi Suzumori, Gen Endo, and Hiroyuki Nabae

Abstract— **As a part of our research on several different types of Giacometti robots, a 20-m-long, considerably light, and simple robot arm, referred to as the Giacometti arm, is developed in this study. Even though the Giacometti arm is not suitable for precise positioning, rapid motion, and high load capacity, which are the aspects most conventional robots focus on, it is designed for extremely specific purposes such as the inspection of otherwise unreachable regions using a small camera at the arm's tip. In addition, it is designed to be essentially safe even if it falls down or hits an object. This aspect is realized using helium-filled balloon bodies and thin pneumatic muscles.**

In this paper, we designed new Giacometti arm which is 20-m-long, weighs 940 g, and has 20 degrees of freedom. To realize this long arm, we derived a kinematic model of the 20-m-long Giacometti arm, factoring in the air resistance. We verified the model using the arm, and its utility was confirmed at a mock-up facility.

I. Introduction

Currently, several types of robots are being developed. Most of them contain rigid linkage mechanisms driven by electric actuators. Even though such robots exhibit high performance and have a number of functions, they are typically heavy and have complicated systems, which makes them difficult to handle and dangerous in cases wherein loss of control occurs. Consequently, it is difficult to put such robots to practical use.

We have proposed "Giacometti robotics" as a new robotics concept [1]. Giacometti robotics was named by ourselves after Alberto Giacometti, a Swiss sculptor. Its ideology is contrary to that of most conventional robots, which focus on high speed, precise positioning, and high load capacity. Giacometti robotics aims to realize robots that are considerably light and simple, easy to handle, and essentially safe by focusing on one important function and neglecting other functions. We have already developed a hexapod Giacometti robot [2], which has considerably long, light, and thin legs. In addition, we have developed a 7-m-long robot arm, which is quite long and light [3]. In this study, we improve the previously developed 7-m-long robot arm, referred to as the "separated type of Giacometti arm with a balloon body (separated Giacometti arm)" and create a new arm referred to as the "welding united type of Giacometti arm with a balloon body (welding Giacometti arm)". We develop a joint model and a kinematic model of the welding Giacometti arm, which includes the effect of air resistance, and verify the models using a prototype of the welding Giacometti arm. The arm is 20-m long, weighs 940 g, and has 20 degrees of freedom (DOFs).

Similar studies of this robot arm can be considered from two viewpoints. The first is an inflatable robot and the second is a disaster response robot. Inflatable robots are being studied as highly safe robots owing to their flexibility and lightness. The robot arms of CMU [4] and CEA [5, 6, and 7] can be considered as types of robot arms. However, when arm length is increased, tension is not transmitted to the tip of the arm owing to friction, and the arm buckles because of the concentrated tension at the base links, as they are driven by a wire. Therefore, these arms are not suitable for lengthening. Festo's robots [8 and 9] utilize the buoyancy of helium; however, their bodies are large and cannot compensate for the weights of incorporated motors and batteries. Thus, they are not suitable for checking narrow spaces. For disaster response robots, the comparison with disaster robots is listed in Table 1. The Giacometti arm is a highly safe robot. Its operation time and noise levels are extremely low as compared to drones. In addition, as it does not scatter dust, it has the advantage that it can be used even on dusty sites.

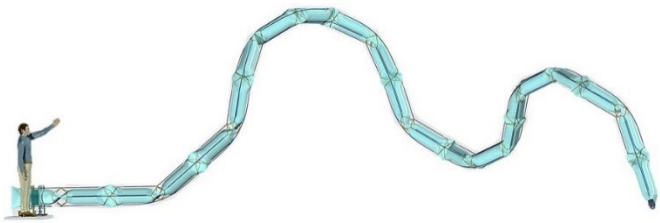

Figure 1. Schematic design of Giacometti arm with balloon body. The arm is considerably long and light and is safe for use around people because of its compliance and lightness.

Table 1 Comparison of Giacometti robots with conventional robots used in disaster affected areas

	Work space	Work time	Safety	Simplicity	Precision	Payload	Low cost
Giacometti arm	☆☆	☆☆☆	☆☆☆	☆☆	☆	☆	☆☆☆
Conventional robot arm	☆	☆☆☆	☆	☆	☆☆	☆☆☆	☆
UAV (drone)	☆☆☆	☆	☆	☆☆☆	☆	☆	☆☆
Crawler type, leg type robot	☆	☆☆	☆	☆	☆☆	☆☆☆	☆

*This research was supported by MEXT KAKENHI (Grant Number 15K13907) under the project "Experimental Proof of Giacometti Robotics Potential".

Masashi Takeichi is with the Department of Mechanical Engineering, Tokyo Institute of Technology, 2-12-1 Ookayama, Meguro-ku, Tokyo 152-8552, Japan (takeichi.m.aa@m.titech.ac.jp).

Koichi Suzumori, Gen Endo, and Hiroyuki Nabae are with the Graduate major in Mechanical Engineering, Tokyo Institute of Technology (nabae@mes.titech.ac.jp)

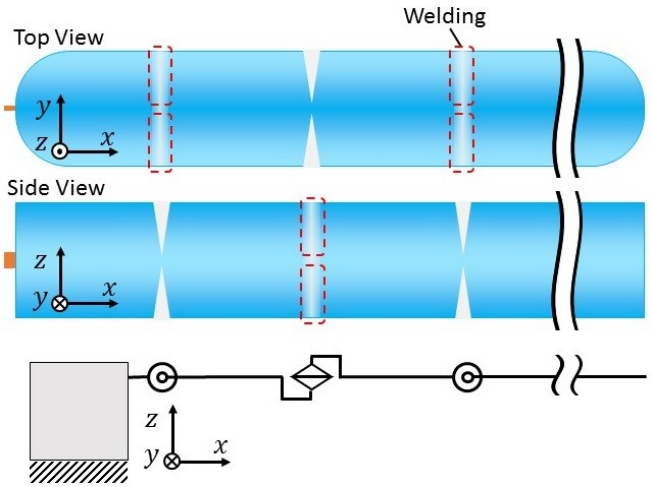

Figure 2. Schematic of arm design. The arm has alternate pitch axes and yaw axes.

Therefore, we developed a robot arm that is light, safe, and long. Two key components helped us realize these requirements. These were, a thin McKibben artificial muscle actuator developed in our laboratory [10] and helium-filled inflatable balloons that compensate for their self-weight. We have already created a 7-m prototype; however, it has the following problems: (1) It requires considerable time to assemble because each link is independent. (2) The movable range is small. (3) The accuracy of the joint angle is low. To counter these, we created a 20-m prototype that overcame these problems and further, conducted experiments at a mock-up facility. In addition, we constructed a kinematic model factoring in the air resistance, which is not considered in heavy and rigid conventional robot arms. We verified the model using the prototype, the image of which is shown in Fig. 1.

II. Design of the Arm

The arm consists of helium-gas-filled polyethylene balloons (link structures), thin McKibben artificial muscles, thin air-feeding tubes, a small camera at the robot arm tip, and cables for the camera. The application of pressure to each artificial muscle drives the arm. For example, the arm can be moved in the upward direction by shrinking the upper-side artificial muscle through applied pressure and expanding the lower-side artificial muscle through decompression.

Inflatable balloons are filled with helium gas to compensate for their self-weight. We use thin McKibben artificial muscles developed in our laboratory [10, 11] as pneumatically driven actuators that have approximately 8 times higher output force-to-weight ratio than conventional commercially available actuators (FESTO DMSP-5). This considerably light muscle is pivotal to realize this extremely long and light arm.

We designed an arm that can carry a CMOS camera (CP-100B, YKmusen, Japan, body weight: 3 g) at its tip. Even though the arm does not work precisely or rapidly, it continues to work even if it hits objects, such as walls and floors, and it is safe even if it falls down because of its high pliability. In addition, the arm rarely causes any damage owing to its flexibility and lightness.

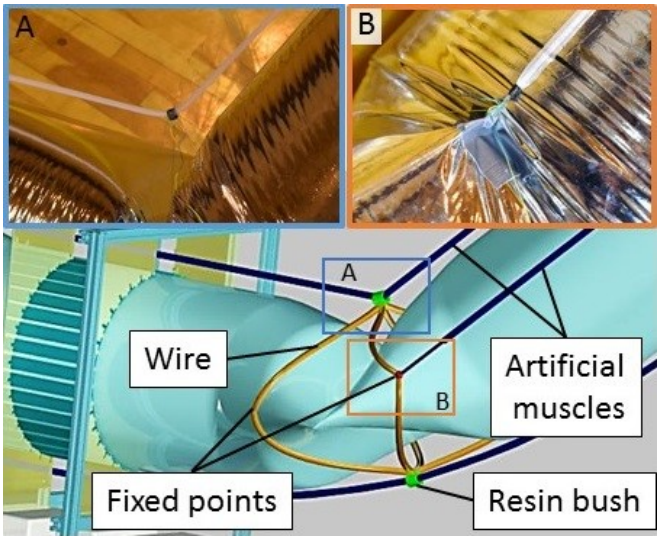

Figure 3. Schematic of the area around a joint. A resin bush (see A) fixes the path of artificial muscle. The fixed point is generated by welding at a spot (see B).

The joint is fabricated by narrowing a balloon using thermal welding. The joint structure is the same as that of CMU's inflatable arm [4]. The pitch and yaw axes are located alternately, and thermal welding is performed while shifting by 90° to generate the axes (Fig. 2). If the links are not welded together at the center of the joint, the gas can freely move back and forth between the links. Therefore, when a gas is injected from the base, it can be simultaneously filled in all the links. Besides, the artificial muscle is fixed using a resin bush at the joint (Fig. 3). As a result, when the joint angle increases, the generated force of the artificial muscle can be efficiently transmitted to the arm to prevent the path length of the inner artificial muscle from becoming too short. The outer artificial muscle is constrained so that it does not deviate from the plane passing through the central axes of the previous and next links. As the resin bush is constrained using static balance of the two wires and artificial muscle, the joint part is considerably lightweight.

III. Modeling

We created two models, i.e., a 20 links kinematic model including the air resistance and a joint model for bending angle control.

A. 20 links Kinematic Model Including Air Resistance

Various models of robot arms have been developed; however, these models do not consider air resistance because conventional robot arms are stiff and sufficiently heavy to neglect the effect of air. However, air resistance has considerable influence on the arm developed in this study because of its extreme lightness and low rigidity. Therefore, a model considering the air resistance was constructed to predict the actual dynamic behavior of the arm.

The proposed model is shown in Fig. 4. We simulated the model using Simulink (MathWorks, Inc.). A link is modeled as a rigid body and an artificial muscle is modeled as a spring whose constant and initial length can change. The joint angle is controlled by changing these parameters. The

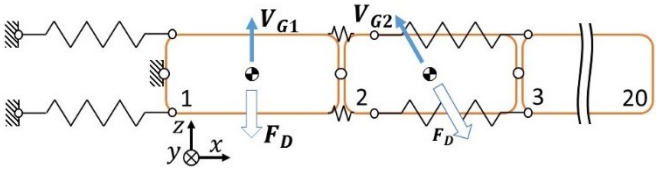

Figure 4. Model considering air resistance. The air resistance according to the center speed of each link is applied to the link.

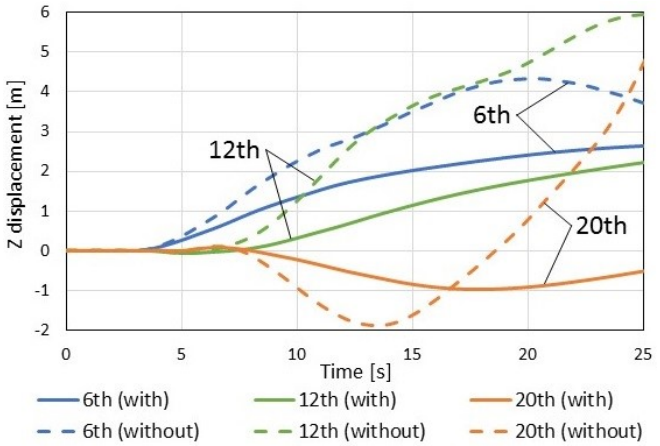

Figure 5. Displacements in the z-axis direction of centers of 6th, 12th, and 20th links in the models with (solid line) and without (dotted line) air resistance.

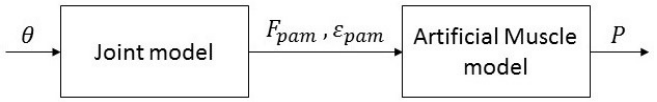

Figure 6. System for controlling the joint angle and the models required for it

pitch axis is balanced by artificial muscles, and the yaw axis is represented by the pitch axis joint and the springs with high spring constants. The air resistance, $\boldsymbol{F_D}$, acting on a cylinder is expressed by (1).

$$\boldsymbol{F_D} = \frac{1}{2}\rho C_D L d |\boldsymbol{V_{Gi}}| \boldsymbol{V_{Gi}} \quad (1)$$

Here, $\boldsymbol{V_{Gi}}$ is the central velocity vector at the i^{th} link, C_D and ρ denote the drag coefficient and fluid density, respectively, L and d denote the length and diameter of the link, respectively. $\boldsymbol{F_D}$ is applied to the center of the link, and the equation of motion is solved in the same manner as that for a normal rigid body model. The displacements in the z-axis direction of the centers of the 6th, 12th, and 20th links in the models with and without air resistance are shown in Fig. 5, when the joint angle of the first joint is changed. It was found that the behavior of the arm varies significantly depending on whether or not air resistance is considered.

B. One Joint Model for Bending Angle Control

It is necessary to set the pressures of the two artificial muscles counteracting each other to appropriate values to control the joint angle. For this purpose, models of joints and artificial muscles are required (Fig. 6). As the model of the artificial muscles had already been developed in [3], we constructed a joint model based on geometry and static mechanics to determine the relation between the shrinkage rate and generated force of the artificial muscle when the joint angle was changed.

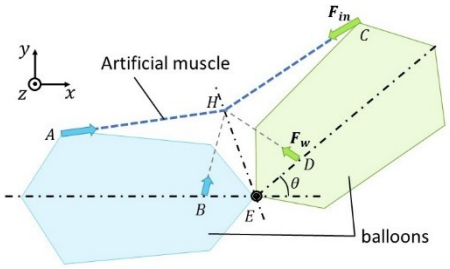

Figure 7. Model showing the path of the artificial muscle that is inside and the balance of forces when the joint is bent.

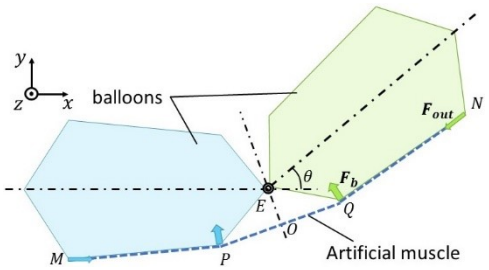

Figure 8. Model showing the path of the artificial muscle that is outside and the balance of forces when the joint is bent.

We considered two cases for the bending of the joint. The artificial muscle was inside (Fig. 7) in the first case and outside (Fig. 8) in the second. The artificial muscle passes through points A, H, and C, as shown in Fig. 7, and through points M, P, O, Q, and N, as shown in Fig. 8. We applied a torque of 0.3 Nm at the joint at all times. In the first case (Fig. 7), the following equations are obtained based on the geometry:

$$AH = (1-\varepsilon)L_{pam}/2 \quad (2)$$

$$BH = L_{wire}/2 \quad (3)$$

where ε and L_{pam} are the contraction ratio and length of the artificial muscle, respectively. L_{wire} is the length of the wire through the resin bush at H, and the wire is connected at both ends of B and D. Based on statics, we obtain the following equations:

$$\boldsymbol{F_{in}} + \boldsymbol{F_w} = t\overrightarrow{AC} \quad (4)$$

$$\boldsymbol{L_{EC}} \times \boldsymbol{F_{in}} + \boldsymbol{L_{ED}} \times \boldsymbol{F_w} = [0 \;\; 0 \;\; 0.3+\alpha]^T \quad (C_y > H_y) \quad (5)$$

$$\boldsymbol{L_E} \times \boldsymbol{F_{in}} = [0 \;\; 0 \;\; 0.3+\alpha]^T \quad (C_y < H_y \quad (6)$$

Here, t is a scalar quantity satisfying (4), α is a correction term obtained from experiments, $\boldsymbol{L_{AB}}$ is a vector from point A to B, and A_y is the y coordinate of point A. In the second case (Fig. 8), we obtain the following equations based on the geometry:

$$MP + PO = (1-\varepsilon)L_{pam}/2 \quad (N_y > P_y) \quad (7)$$

$$MO = (1-\varepsilon)L_{pam}/2 \quad (N_y < P_y) \quad (8)$$

The following equations are obtained based on the static mechanics:

$$\boldsymbol{F_b} = \boldsymbol{F_{out}} \times \left(\frac{\boldsymbol{L_{QN}}}{QN} + \frac{\boldsymbol{L_{QP}}}{QP}\right) \quad (9)$$

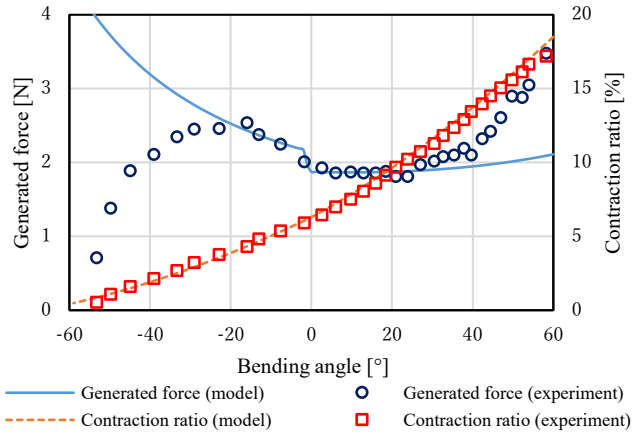

Figure 9. Relationships between the bending angle, the contraction ratio and the generated force obtained from the model and experiment, when a torque of 0.3 Nm is applied to the joint.

$$\boldsymbol{L_{EN}}\times\boldsymbol{F_{out}} + \boldsymbol{L_{EQ}}\times\boldsymbol{F_b} = -[0\ \ 0\ \ 0.3+\beta]^T \quad (N_y > P_y) \qquad (10)$$

$$\boldsymbol{L_{EN}}\times\boldsymbol{F_{out}} = -[0\ \ 0\ \ 0.3+\beta]^T \quad (N_y < P_y) \qquad (11)$$

Here, β is the correction term obtained experimentally. The contraction ratio, ε, and generated forces, F_{in}, F_{out}, of the artificial muscle obtained from these models are shown in Fig. 9, in which α and β are 0.

We conducted an experiment to investigate the relationship between the bending angle, the contraction ratio, and the generated force when a torque of 0.3 Nm was applied to the joint by hanging a weight on the balloon. The results of the experiment are shown in Fig. 9. The values of contraction ratio obtained from the model and the experiment are in agreement. However, there are a few points where the values of generated force obtained from the model and experiment are different. The discrepancies observed at angles ranging from approximately 40° to 60° result from the interference between the balloons. This effect is also observed at angles ranging from -60° to -40°. Considering the resistance force due to balloon interference, it is necessary to reduce the output force of the outer artificial muscle and increase the output force of the inner artificial muscle. By connecting the whole smoothly, it approached actual behavior. The following heuristic equations show the added correction term:

$$\alpha = 0.03\ (0 \le \theta \le 40)$$
$$\alpha = 0.03 + (\theta - 40)^2/1600\ \ (40 \le \theta)$$
$$\beta = 0.01\times(1-\theta/2)\ \ (-2 \le \theta \le 0)$$
$$\beta = -0.3\times(\theta - 20)^2/1600\ (\theta \le -20)$$

The result for the modified model is shown in Fig. 10. It was possible to change the joint angle by applying an appropriate pressure according to the contraction ratio and generated force calculated from the constructed model.

IV. Experiments

A. Experiment with 1-link Arm

To verify that the modeling described in Section III is correct, we created a 1-link model and investigated the relationship between the command angle and actual angle (Fig. 11). Two markers were placed on the arm and their

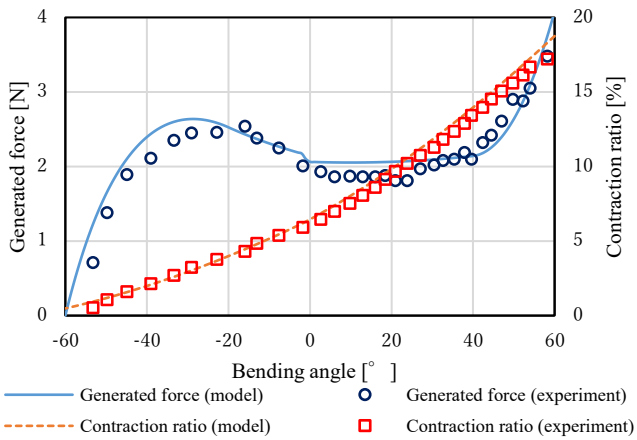

Figure 10. Relationships between the bending angle, the contraction ratio, and the generated force obtained from the modified fixed model and experiment, when a torque of 0.3 Nm is applied to the joint.

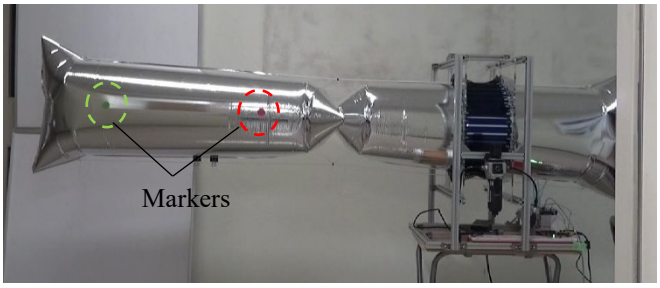

Figure 11. 1-link model to verify the joint model.

coordinates were detected to measure the joint angles. First, we move the bending angle in the 1-link model from 0° to 60°, 60° to -60°, and -60° to 0° as preparatory movements. Then, we perform the same action quasi-statically and measure the actual angle. The command angle changes by 1° every 5 sec; however, it changes by 1° every 20 sec between -30° to 30° because the angle tends to change significantly around the 0° point, which is a singularity point. The results of the experiment are shown in Fig. 12. A movable range of 60° to -60° was confirmed. However, a maximum error of approximately 30° and an average error of approximately 11° were observed between the command and measured values. In addition, hysteresis at the time of reciprocation was observed. The reason for the large change near 0° can be that the link is distorted by the compression force of the artificial muscle because it is softer than the conventional link mechanism. The hysteresis property was confirmed because the artificial muscles, along with the film balloons exhibit this property as the structural material. Controls based on the Preisach, play, and stop models are primarily considered to govern the hysteresis characteristics of a system [12 and 13]. However, these controls are computationally expensive. Even though it is possible to predict the measured value from the command value, feedback control is required to set the angle to an arbitrary value. As a result, the calculation time increases further. For this reason, in this study, the system is control by sending the value that is modified in advance, based on the measured value as the command value. For example, when a command value of 13° is ordered at the present stage, it is assumed that

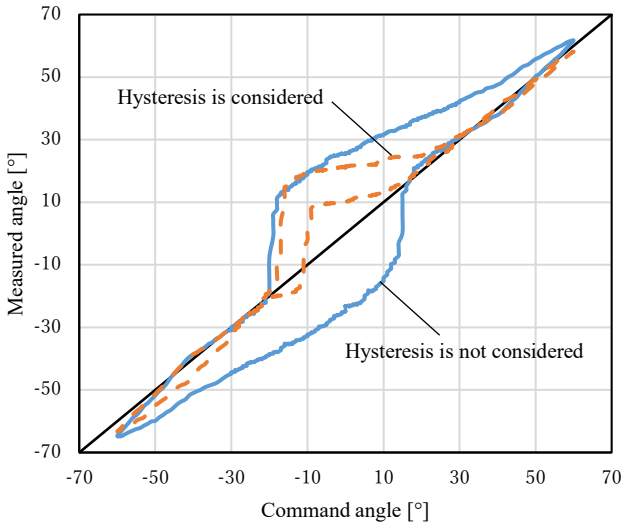

Figure 12. Relationship between measured and command values relative to consideration of hysteresis.

an actual value of 30° is obtained. In the control considering hysteresis, a command value of 13° is sent to the arm when a command value of 30° is required. Then, an actual value of 30° is obtained. The expression related to this control is given below.

$$E(\theta) = \xi F(\theta) + (1 - \xi)T(\theta) \qquad (12)$$

Here, θ is the command value ordered from a PC, $E(\theta)$ is the actual command value sent to the arm, $F(\theta)$ is the correction angle based on the measured value when changing the joint angle from -60° to 60°, $T(\theta)$ is the correction angle based on the measured value when changing the joint angle from 60° to -60°, and ξ is the transition coefficient, which varies depending on the history of the input, θ. The experimental results for the 1-link model obtained using control considering the hysteresis property are shown in Fig. 12. The experimental conditions are the same as that in the case in which hysteresis was not considered. Even though there was almost no difference between the maximum errors for the two experiments, the average error for control considering hysteresis was less than half of that for control without hysteresis. The utility of control considering hysteresis was confirmed. Particularly, the command and measured values at -60° to -20° and 20° to 60° nearly agree with each other, which indicates that this type of control works effectively. Offsets are added to the angles obtained from videos to minimize average errors. The purpose of adding offsets is to neglect the influence of the inclination of the camera used to acquire an image, the inclination of the base, and the inclination between the base and the base link fixed to it.

B. Experiment with 20-link Arm

As we succeeded in controlling the joint angle using the 1-link model, we extend the model to 20 links and use it to confirm the motion at the mock-up facility (Naraha Remote Technology Development Center) (Fig. 13). The mockup facility is indoors; however, there was slight airflow due to air conditioning. As it was confirmed that the tip of the arm

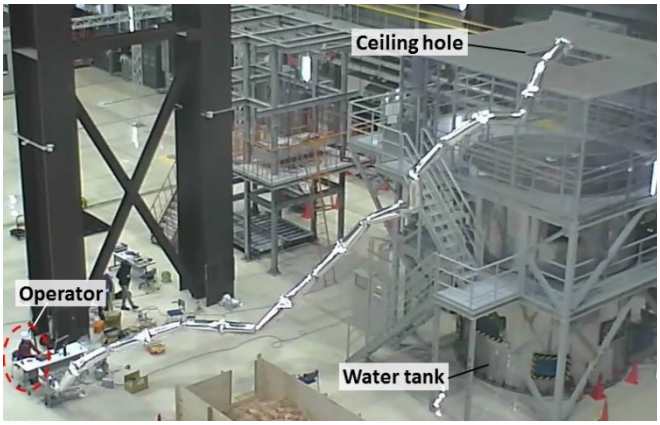

Figure 13. Mock-up facility of energy plant (Naraha Remote Technology Development Center), where experiments were conducted for inspecting the interior of a water tank building through ceiling holes, using the 20-link arm.

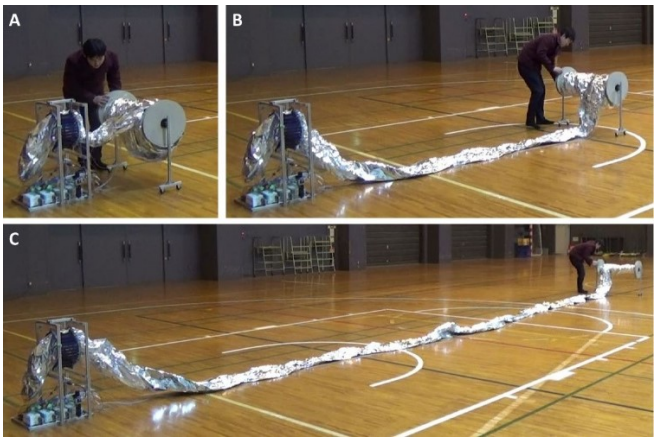

Figure 14. Expanding the arm from wound state in a roll (A) to expanded state (C).

Figure 15. Injecting helium gas into the arm. Helium gas is injected from an inlet port on the base balloon to all balloons through narrow ports between the balloons. 23 min were required from starting (A) to full injection (C).

was undulating at a speed of approximately 0.2 m/s, it is considered that the airflow had the same speed. The length of the arm and buildings at the mock-up facility were measured using a 3D scanner (FARO LASER SCANNER FOCUS 3D X 130, FARO, USA). The experiment and results are described below.

In the mock-up facility of the energy plant, we first confirmed whether the arm could work by injecting gas from the state wherein the balloon did not have any gas inside. Fig. 14 shows the manner in which the arm is deployed from the folded state, and Fig. 15 shows the state of the experiment in which the gas is injected from the state where it is not injected inside. Approximately 23 min were required to inject the gas into all the links. As it is difficult to adjust the buoyancy of the arm, we attached weights on each link to

Table 2 Specifications of Giacometti arm and previously developed arm.

	length	diameter	weight	DOF	Movable range	Weight / length
Giacometti	19.8 [m]	300 [mm]	940 [g]	20	±60 [°]	47 [g/m]
CAE [10]	3 [m]	200 [mm]	500 [g]	3	±80 [°]	167 [g/m]

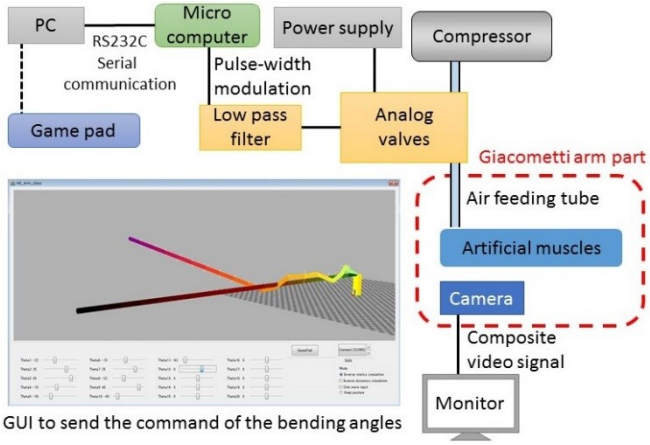

Figure 16. Schematic of the arm system and GUI to control the arm.

balance the buoyancy of helium and the gravity of each link. The specifications of this arm and a previously developed arm are listed in Table 2.

We performed an experiment to observe the interior of a water tank building through a celling hole to confirm whether the arm is useful for observation. The height of the tank building is 8.5 m, the distance from the base of the arm to its ceiling window frame is 14 m, and the ceiling window frame measures 2 m × 2 m. The arm system is shown in Fig. 16. The 20-link arm is operated using the GUI on a PC or a game pad connected to a PC. We observed the interior of the building through holes in the ceiling and manipulated the arm based on visual feedback. We succeeded in reaching the target point and observing the interior (Fig. 17), for which approximately 12 min were required. Contact between the arm and structure occurred; however, they were not damaged owing to the compliance and flexibility of the arm.

C. *Comparison between Model with Air Resistance and Experiment*

We verified that the model considering air resistance is correct using the 20-link arm. Using a video, we estimated the displacement for each link when the base joint is bent. The motion of the 20-link arm is shown in Fig. 18. Fig. 19 shows the comparison of the results obtained by performing the same operation in the model and experiment. Table 3 shows the concordance rates between experiment and model. The concordance rates are the average values of $1 - |X_m - X_e|/|X_e|$ calculated every 0.1 sec from 10 sec to 25 sec. Here, X_m and X_e represent the displacement of the model and experiment. The results obtained from the model and experiment are in agreement, and the utility of the model can be confirmed. There is a discrepancy between the values obtained from the model and experiment after 15 sec. This is because the joints of the prototype do not return completely to 0° owing to hysteresis, while the joints in the model return completely to 0°.

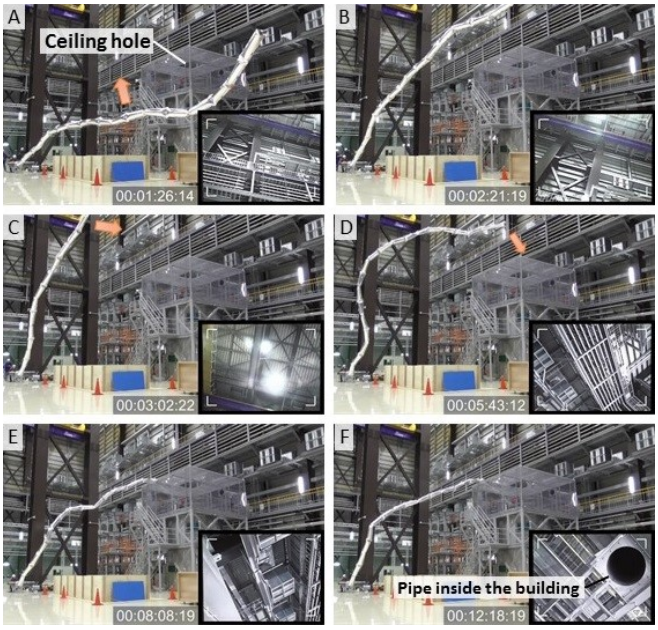

Figure 17. Inspection test inside the water tank facility using the 20-m Giacometti Arm. The inset image shown at the bottom right part of each photo is from the camera mounted at the arm tip. The arm moves upward (A)-(B) and approaches the celling hole (C)-(D). Two tip balloons touch the housetop of the water tank facility (E). The arm and housetop are not damaged owing to the essential safety of Giacometti arm. The arm tip successfully enters the celling hole and obtains the image of the pipe inside it (F). The test is conducted at Naraha Remote Technology Development Center.

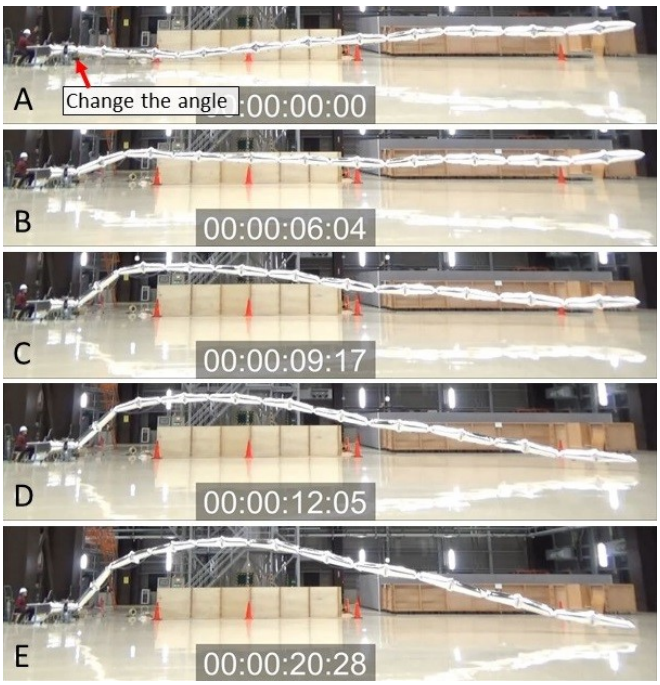

Figure 18. Experiment to verify the model considering air resistance using the 20-link arm.

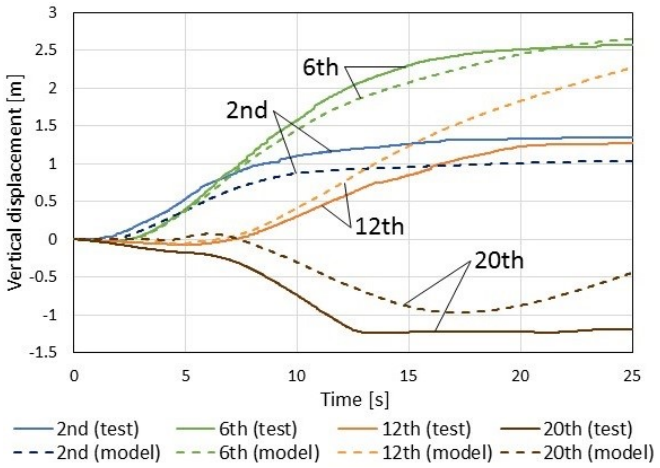

Figure 19. Comparison of results obtained by performing the same operation in the model and experimentally.

Table 3 The concordance rates between the experiment and model.

Link number	2nd	6th	12th	20th	Average
With air resistance	77 %	94 %	51 %	62 %	71 %
Without air resistance	78 %	32 %	-99 %	-190 %	-45 %

V. Conclusion

By combining thin artificial muscles and helium-filled balloons, we developed a welding Giacometti arm based on Giacometti robotics. We modeled, developed, and evaluated the extremely long and light robot arm that can observe locations that a conventional robot arm cannot reach. The primary findings of this study are given below.

a) Development of 20-m-long Giacometti arm with a balloon body

We developed a considerably light, safe, and simple Giacometti arm using thin artificial muscles with high force/weight ratio, which is significantly higher than that of a conventional actuator. We demonstrated that the arm is an extremely safe robot arm that causes almost no harm to people and surroundings even if the arm is deemed uncontrollable due to malfunction or mishandling. Moreover, this arm is considerably longer than previously developed robot arms. We succeeded in observing the interior of an 8.5-m high water tank building from ceiling holes, and thereby demonstrated the superiority of the long-length arm.

b) Modeling of a Giacometti arm with a balloon body

We constructed a model considering air resistance, which is not considered in conventional robot arms. The results of the experiment conducted using the prototype and those of the model considering air resistance agreed with 71%, whereas in the model without air resistance agreed with -45%. As a result, it was confirmed that the behavior of the robot arm could be reproduced by the model considering air resistance. Additionally, we constructed a joint model and verified the validity of the model using the 1-link arm. In future, we will conduct experiments using the robot arm and incorporate the control in the model.

References

[1] K. Suzumori, "New pneumatic artificial muscle realizing Giacometti robotics and soft robotics," in *6th Int. Conf. Manufacturing, Machine Design and Tribology (ICMDT 2015)*, Okinawa, Japan, 2015, pp. 4–5.

[2] S. Kurumaya, F. Ni, and K. Suzumori, "Design of hexapod Giacometti robot with very long, light, and thin legs," in *Proc. 6th Int. Conf. Advanced Mechatronics (ICAM2015)*, Tokyo, Japan, 2015, pp. 136–137.

[3] M. Takeichi, K. Suzumori, G. Endo, and H. Nabae, "Development of Giacometti arm with balloon body," *IEEE Robotics and Automation Letters*, vol. 2, no. 2, Apr. 2017, pp. 951–957.

[4] S. Sanan, M. H. Ornstein, and C. G. Atkeson, "Physical human interaction for an inflatable manipulator," in *33rd Annu. Int. Conf. IEEE EMBS*, Boston, Massachusetts, USA, 2011, pp. 7401–7404.

[5] S. Voisembert, A. Riwan, N. Mechbal, and A. Barraco, "A novel inflatable robot with constant and continuous volume," in *IEEE Int. Conf. Robotics and Automation*, Shanghai, China, 2011, pp. 5843–5848.

[6] S. Voisembert, N. Mechbal, A. Riwan, and A. Aoussat, "Design of a novel long-range inflatable robotic arm: Manufacturing and numerical evaluation of the joints and actuation," *J. Mech. Robotics*, vol. 5, no. 4, pp. 045001, Oct. 2013.

[7] Robotics in Video, 2013. [Online], Available: http://derobotica.blogspot.jp/2013/01/long-range-inflatable-robot-arm.html#.V7vewPntlBc, Accessed on: Aug. 23, 2016.

[8] Air_ray Festo Corporate, Sankt Ingbert, Germany, 2007. [Online], Available: https://www.festo.com/group/en/cms/10245.htm, Accessed on: Dec. 2, 2016.

[9] AirPenguins Festo Corporate, Sankt Ingbert, Germany, 2009. [Online], Available: https://www.festo.com/group/en/cms/10242.htm, Accessed on: Dec. 2, 2016.

[10] M. Takaoka, K. Suzumori, S. Wakimoto, K. Iijima, and T. Tokumiya, "Fabrication of thin McKibben artificial muscles with various design parameters and their experimental evaluations," in *5th Int. Conf. Manufacturing, Machine Design and Tribology (ICMDT 2013)*, Busan, South Korea, 2013, pp. 82.

[11] S. Kurumaya, K. Suzumori, H. Nabae, and S. Wakimoto, "Musculoskeletal lower‐limb robot driven by multifilament muscles," *Robomech Journal*, Springer Open, vol. 3, no. 18, Sep. 2016.

[12] G. Bertotti, "Dynamic generalization of the scalar Preisach model of hysteresis," *IEEE Trans. Magn.*, vol. 28, no. 5, pp. 2599–2601, Aug. 2002.

[13] S. Bobbio, G. Milano, C. Serpico, and C. Visone, "Models of magnetic hysteresis based on play and stop hysterons," *IEEE Trans. Magn.*, vol. 33, no. 6, pp. 4417–4426, Aug. 2002.